(Received 26 September 2025, Accepted 8 December 2025, Scheduled 22 December 2025)

Research on RIS-Assisted Millimeter Wave Beam Tracking Algorithms for Vehicular Communications

Chenwei Feng*, Zhenzhen Lin, Yawei Sun, Yu Sun, Yangbin Huang, and Yinhua Wu

School of Opto-electronic and Communication Engineering, Xiamen University of Technology, Xiamen 361000, China

ABSTRACT: In this paper, for millimeter wave (mmWave) vehicle-to-infrastructure communication, a reconfigurable intelligent surface (RIS) is introduced for assisted beam tracking in order to overcome the problem that the line-of-sight (LOS) transmission characteristics of mmWave are highly susceptible to communication disconnection caused by large vehicles or obstacles in a highly mobile scenario like Internet of Vehicles (IoV). In this paper, we study the case of switching to the RIS-assisted virtual-line-of-sight (VLOS) path for temporary beam tracking when the direct connection LOS path is disconnected. The cascading channel model for the VLOS path used for tracking after the introduction of RIS is investigated. Combining the new state model of position and velocity, a three-dimensional beam tracking model of the VLOS path is derived based on the extended Kalman filter algorithm. The beam tracking process is designed, and the beam tracking performance is analyzed for different cases under this scheme. Simulation results show that the scheme in this paper has lower tracking error than the scheme of the conventional state model, and the introduction of RIS can overcome the problem that mmWave IoV communication is vulnerable to occlusion.

1. INTRODUCTION

MmWave technology offers abundant spectrum resources and extremely high data transmission rates, making it highly suitable for the low-latency requirements of IoV scenarios. However, the characteristics of mmWave technology and the complex communication environment of IoV impose multiple constraints on its application [1–3]. Compared to low-frequency signals, mmWave transmission suffers higher losses and is easily absorbed by the atmosphere and rain, thereby reducing the effective communication range. Although mmWave antennas with small dimensions can be configured into multiple-input multiple-output (MIMO) arrays and form directional beams through beamforming techniques, the high-speed movement of vehicles induces significant Doppler shifts and rapid channel changes [4], thereby reducing communication reliability. More importantly, mmWave signals cannot penetrate most solid objects, and their transmission typically relies on LoS paths. In high-speed IoV scenarios, obstacles such as vehicles and buildings can easily cause LoS link interruptions. Therefore, how to achieve stable beam tracking in mmWave IoV to ensure communication quality is a critical issue that urgently needs to be addressed.

For high-speed mobile users within the communication range, it is necessary to predict and adjust the communication beam for the next time slot at the current time slot to track their time-varying channels. This method is referred to as beam tracking [5–7]. Communication beams formed by mmWave MIMO systems are extremely sensitive to directional changes. Even slight angular deviations of vehicles or environmental variations can cause beam misalignment or even link disruption. In particular, under time-varying channels, insufficient beam alignment accuracy increases the number of channel re-estimations, resulting in significant system overhead. Therefore, in mmWave IoV scenarios, highly mobile communications require low-error beam tracking methods to ensure continuous and stable link performance. Meanwhile, due to mmWave being susceptible to shadowing, conventional beam tracking is easily obstructed by large vehicles or obstacles in high-speed moving environments, further complicating implementation.

RIS serves as a low-cost, low-complexity, and easily deployable auxiliary communication technology, providing an effective solution to communication challenges in mmWave IoV. RIS typically consists of a large number of controllable electromagnetic elements. By adjusting their amplitude, phase, polarization, or frequency characteristics, dynamic control of spatial signals can be achieved [8–10]. RIS as an application of metamaterials is not only easy to deploy at scale but also cost-effective, offering a novel solution to address communication challenges in mmWave IoV. The introduction of RIS technology transforms traditional wireless communication from passive channel adaptation to active signal modulation, thereby establishing Smart Radio Environments (SRE) [11]. This approach provides a novel technical pathway for addressing challenges in mmWave communication, such as obstruction and Doppler effects. In [12], researchers investigated an intelligent metasurface-assisted Mobile Edge Computing (MEC) system for ultra-high-reliability, low-latency communication based on a digital twin-driven framework. Simulation results indicate that compared to traditional MEC systems, this RIS-assisted MEC system can reduce transmission latency and energy con-

* Corresponding author: Chenwei Feng (cwfeng@xmut.edu.cn).

sumption. In [13], the research focuses on the design of dynamic wireless networks supported by multiple RISs. The study constructs a long-term system update framework and addresses a dynamic optimization problem. Simulation results demonstrate that this design enhances user fairness across various dynamic scenarios while maintaining the supply-demand balance better in resource allocation.

In multi-user, highly interactive scenarios such as the IoV, the communication environment is complex, and communication links are prone to obstruction. Benefiting from the advantages of passivity, low cost, and easy deployment, RIS can be deployed at key locations to assist communication. By adjusting the reflection angles of the RIS, a new Base Station-RIS-User Equipment (BS-RIS-UE) transmission path can be established when the LOS link is blocked, thereby mitigating the communication interruption of mmWave signals caused by obstruction. RIS-assisted cascaded channels consist of two segmented subchannels: Base Station-RIS (BS-RIS) and RIS-User Equipment (RIS-UE) [14]. The introduction of RIS provides a solution for severe Doppler effects in high-speed mobile scenarios [15]. By manually adjusting the signal amplitude and phase in real time, it is possible to effectively suppress the severe fluctuations in received signal strength caused by Doppler shift. Although RIS augmentation can mitigate some adverse effects generated by mmWave IoV systems to a certain extent, sustained and stable high-speed mobile communications still require efficient beam tracking methods tailored for dynamic scenarios.

There are three general types of approaches to the implementation of beam tracking technology [16, 17]: (1) training-based beam tracking; (2) dynamic filtering principle-based beam tracking; (3) sensor fusion-based beam tracking. Each of the different beam tracking types has its own characteristics. Training-based beam tracking maintains beam collimation by periodically training beam direction information. Since the channel change rate is more frequent in dynamic communication scenarios, frequent training is required, which generates a large system overhead. Sensor fusion-based beam tracking typically utilizes sensors such as the Global Positioning System (GPS) or radar to obtain state information to aid in beam alignment. However, this method is very sensitive to the environment and brings a certain time delay, which has more limitations for high-speed moving IoV scenarios. In contrast, beam tracking based on the dynamic filtering principle mainly uses an iterative prediction method with a lower system overhead and fewer limitations. This is the tracking method that is focused on in this paper.

The common dynamic filtering algorithms are Kalman filter (KF), extended Kalman filter (EKF), unscented Kalman filter (UKF), particle filter (PF), etc. [17]. The trajectory of mobile users in IoV is limited by road conditions and traffic rules, and there will be certain regularity, and their continuous motion makes the prediction simpler. The EKF algorithm has a better tracking effect for this simple nonlinear system.

EKF-based filtering schemes are proposed in [18–20]. In [18], an EKF tracking algorithm based on the second-order Taylor expansion is proposed. In exchange for the improvement of beam tracking accuracy, the computational complexity is increased, and some time delay is sacrificed. In [19], a robust beam tracking method is proposed for dynamic scenes where the mmWave beam is sensitive to angle changes that can lead to a dramatic degradation in signal quality. A joint iteration based on the Minimum Mean Square Error (MMSE) and the EKF algorithm is performed. In [20], an iterative approach is used to comprehensively scan the available beam combinations so as to construct a measurement matrix suitable for EKF.

Ref. [21] differs from [20] in that only one measurement is used to track the angle change thus reducing the system overhead. Although the scheme in [21] reduces the system overhead, the choice of using the EKF to track a highly nonlinear system leads to a more complicated linearization process of the Jacobi matrix solution, further making the dynamic tracking performance slightly worse. This problem is further validated by a study in [22], which concluded that the current system model is not applicable to mmWave vehicle communication. The amount of angle change during tracking is nonlinear with respect to the angle. Since the assumed noise generated by the speed variation is nonadditive, using angle as a state variable would increase the computational complexity of the Jacobi matrix of the EKF algorithm significantly. Therefore, this literature uses position, velocity and channel gain as state variables to provide a linear state model and additional process noise for vehicle communication. The validation shows that this approach improves beam tracking with lower computational complexity by considering the motion characteristics of the system. However, the scheme is only based on the two-dimensional scenario under MIMO, which is not quite suitable for the actual application scenario. In [23], position and velocity are used as tracking variables and a three-dimensional (3D) scene model is constructed. A small number of vehicle motions is fed back to the road side unit (RSU) using uplink measurement signals to predict the vehicle motion states in a high mobility scenario. Although this literature discusses a 3D scenario, it is limited to discussing only the Multiple Input Single Output (MISO) scenario considering the complexity.

In [24], the study focuses on the estimation of the downlink direct channel and downlink cascaded channel in RIS-assisted Frequency Division Duplexing (FDD) MIMO system. The time-varying channel is described by a Gauss-Markov model. A KF-based two-stage training algorithm for direct and cascaded channel tracking is designed, and the estimation errors are reduced by optimizing the design of the guide and reflection coefficient matrices. However, this scheme is more complex and may not meet the requirements of low-latency tracking for IoV communication. In [25], the user localization and tracking problems in a downlink MIMO system are studied, where multiantenna BS and multiple RISs are deployed to assist in the localization and tracking of multiantenna users. A probability transition model of user movement is developed. Based on a factor-graph representation of the probability model, a message-passing algorithm called the Bayesian user localization and tracking algorithm is developed to estimate and track user location and angle of arrival in an online fashion. The study is more applicable to users moving slowly and may

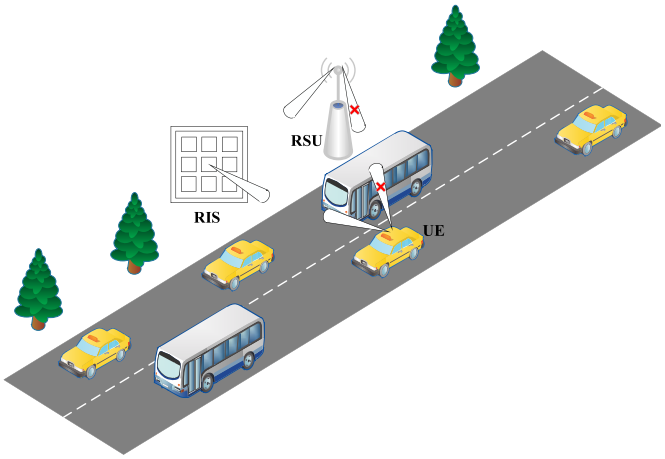

FIGURE 1. Scenario model.

not be applicable to tracking users of vehicles moving at high speeds. A time-varying RIS-assisted mmWave system is studied in [26]. A robust complex-valued EKF method is proposed to solve the beam alignment problem. In order to simplify the model, the RIS in this paper uses a Uniform Linear Array (ULA) array, which obviously has significant limitations. In addition, the paper still uses angle and gain as the state model for EKF tracking in mobile communication, which will increase the computational complexity of the Jacobi matrix and degrade the tracking performance.

In this paper, RIS is introduced in a mmWave vehicle-to-infrastructure (V2I) scenario to assist communication. A new state model combining position and velocity based on the EKF algorithm is investigated for 3D VLOS beam tracking. The contributions of this paper are summarized as follows.

(1) To address the issue of mmWave IoV communication links potentially being obstructed by large vehicles or obstacles in real-world scenarios, this paper introduces an RIS in V2I scenarios. It constructs a BS-RIS-UE VLOS transmission path to replace the obstructed direct link. Furthermore, by addressing the issue of angular deviation during vehicle motion, a VLOS beam tracking process more closely aligned with real-world three-dimensional vehicle networking environments was designed, thereby overcoming the limitations of existing research that predominantly relies on two-dimensional plane modeling.

(2) The introduction of RIS constitutes two new segmented subchannels, BS-RIS and RIS-UE. The deployment of RIS in mmWave systems to track further increases the difficulty of beam alignment. In order to keep the beam alignment between transceivers and maintain the existence of VLOS paths, a detailed study of the cascaded channel model and the transmission signal model of the RIS-assisted VLOS path in the scenario of this paper is carried out.

(3) Traditional EKF methods employing angle and gain as state variables are unsuitable for high-speed IoV scenarios. Their complex Jacobian matrix solutions and strong nonlinearity make it difficult to meet real-time requirements. To this end, this paper employs position and velocity as state variables, which better align with vehicle motion characteristics, to construct a VLOS beam tracking model for three-dimensional MIMO scenarios. This approach significantly reduces the linearization complexity of the EKF while maintaining tracking accuracy. Simulation analysis evaluates the tracking performance of this model under various conditions.

The rest of this paper is organized as follows. In Section 2, the scenario and system model of this paper are described in detail. In Section 3, the overall beam tracking process for this scenario is designed. The beam tracking of the VLOS path is also derived, and the EKF is introduced. Simulation analysis is performed in Section 4. Section 5 concludes the whole paper.

Notation: $\mathbf{A}$ represents a matrix; $\mathbf{a}$ denotes a vector; and a is a scalar. $\mathbf{A}^{\mathrm{T}}$, $\mathbf{A}^{*}$, $\mathbf{A}^{\mathrm{H}}$, $\mathbf{A}^{-1}$ and $\|\mathbf{A}\|^2$ respectively denote the transpose, conjugate, conjugate transpose, inverse, and magnitude of $\mathbf{A}$. $|a|$ denotes the absolute value of a. $E[\cdot]$ is the expected value. $\mathbf{I}_M$ is the $M \times M$ identity matrix. $\mathcal{CN}(m, \sigma^2)$ means a complex Gaussian random variable with mean of m and covariance of σ^2.

2. SYSTEM MODEL

2.1. Scenario Model

This paper focuses on the downlink communication of VLOS paths in the mmWave V2I scenario. A one-way two-lane VLOS scenario is considered, in which RIS-assisted communication is introduced. The scenario model is shown in Fig. 1. The roadway is continuously covered by a single RSU with RIS-assisted communication deployed within the coverage area. The coverage allows vehicle users to communicate directly via the BS-UE path, as well as temporarily via the BS-RIS-UE path when the BS-UE path is blocked [27–30]. The RSU can communicate with multiple vehicle users in range at the same time within the coverage area, and use beam tracking technology to continuously track to guarantee the stability and accuracy of the communication link. Both RSUs and vehicle users are equipped with MIMO antennas for signal reception and transmission [31]. The RIS is a passive device that does not have the ability to transmit, receive, or process the pilot signal, but only the reflection function [32]. Thus, the power allocation problem of RIS is not studied in this paper. In the scenario of IoV, the sharing of state information between terminals enables the RSU to predict the vehicle trajectory more accurately and reduces the overhead, without requiring frequent updates. In this case, if the LOS path is disconnected due to an emergency, it can be quickly switched to the RIS-assisted VLOS path for temporary communication. The vehicle users in the scenario periodically broadcast their own status information, including vehicle position, speed, and safety information to other nearby IoV users and RSU, so as to ensure that RSU can make reasonable predictions about the vehicle's motion trajectory and achieve continuous and stable beam tracking.

2.2. Transmission Model

This paper focuses on the RIS-assisted downlink V2I communication process, mainly on the beam tracking process of switching to the VLOS path of BS-RIS-UE when the LOS path is blocked and disconnected. Due to the concentrated energy of

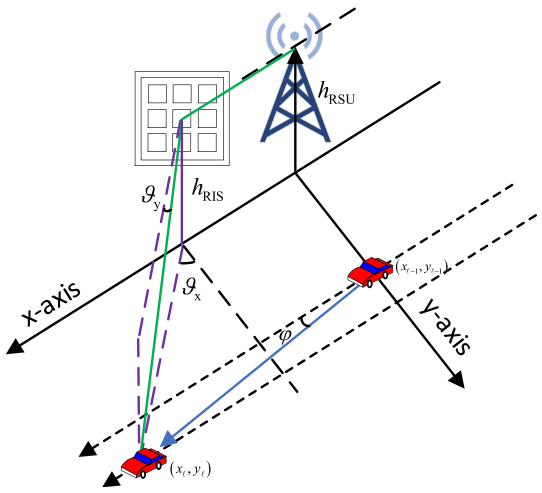

FIGURE 2. Research model.

mmWave beams, they are highly resistant to interference and are very little influenced by neighboring beams. Then, to simplify the model and assuming that the influence of other beams is negligible, the study object can be simplified to a single RSU communicating with a single vehicle user through a single RIS reflection. It is important to note that RIS can be deployed at scale in practical applications. Better performance can be achieved by selecting the right RIS at the right location. In the study scenario of this paper, only the case of a single RIS reflection is considered. The research model is shown in Fig. 2. The coordinate system is constructed with the RSU as the origin, the forward direction of the vehicle as the x-axis, and the vertical direction of the forward direction as the y-axis. The RIS exists within the coverage of the RSU and reflects the communication beam.

Both the transmitter and receiver are built based on a MIMO system. The hybrid beamforming scheme is used in this scenario because of the relative superiority of the hybrid architecture that can balance performance and cost [33, 34]. Since only a single communication link is studied in this paper, only one RF chain at each end is assumed to simplify the model. For the generality of the study, common ULA arrays are used at the transceiver end. The number of antennas at the transceiver is N_{UE} and N_{BS}, respectively. RIS has the special feature that it is a device in which the electromagnetic units are arranged uniformly in a plane, and in general it is arranged using Uniform Planar Array (UPA) arrays [35–37]. Let its array have N_x rows and N_y columns, then the array element size of a UPA array is $N_{\mathrm{RIS}} = N_x N_y$. The array element spacing in this scenario all satisfy $d = \lambda/2$. According to the hybrid beamforming scheme, the data symbol s is precoded in the digital domain and analog domain successively through the beamformer $\mathbf{f} \in \mathbb{C}^{N_{\mathrm{BS}}}$ at the transmitter. After passing through the RIS cascaded transmission channel, it is then received at the receiving end by the combiner $\mathbf{w} \in \mathbb{C}^{N_{\mathrm{UE}}}$. The beamformer and the combiner satisfy $\|\mathbf{f}\|^2 = 1$ and $\|\mathbf{w}\|^2 = 1$. Then the received signal at the discrete time ℓ can be expressed as

$$r_\ell = \sqrt{\rho_\ell}\mathbf{w}^{\mathrm{H}}\mathbf{H}_\ell\mathbf{f}s + \mathbf{w}^{\mathrm{H}}\mathbf{n}_{\mathrm{AWGN}} = \sqrt{\rho_\ell}\mathbf{w}^{\mathrm{H}}\mathbf{H}_\ell\mathbf{f}s + n_\ell \quad (1)$$

where ρ_ℓ is the average Signal-to-Noise Ratio (SNR), $\mathbf{H}_\ell \in \mathbb{C}^{N_{\mathrm{UE}} \times N_{\mathrm{BS}}}$ here denotes the cascaded channel matrix of BS-RIS-UE, and $\mathbf{n}_{\mathrm{AWGN}} \in \mathbb{C}^{N_{\mathrm{UE}}}$ is the additive complex Gaussian white noise with zero-mean. By assuming a unit antenna gain at the transceiver, the average SNR can be expressed as

$$\rho_\ell = \frac{p}{\sigma_n^2}\left(\frac{\lambda}{4\pi d_\ell}\right)^n \quad (2)$$

where p is the transmitted power, σ_n^2 is the noise power, λ is the wavelength, d_ℓ is the distance of the VLOS path, and n is the path loss index.

Saleh-Valenzuel mmWave channel model is commonly used in mmWave channel modeling [38]. There are two segmented subchannels, BS-RIS and RIS-UE in the BS-RIS-UE cascaded channel. Disregarding the multipath case, their time-varying channel models are expressed as

$$\mathbf{H}_{\mathrm{RB}} = \mathbf{a}_{\mathrm{RIS}}\left(\bar{\vartheta}_x, \bar{\vartheta}_y\right)\beta_{\mathrm{RB}}\mathbf{a}_{\mathrm{BS}}^{\mathrm{H}}\left(\psi_{\mathrm{BS}}\right) \quad (3)$$

$$\mathbf{H}_{\mathrm{UR},\ell} = \mathbf{a}_{\mathrm{UE}}\left(\psi_{\mathrm{UE},\ell}\right)\beta_{\mathrm{UR},\ell}\mathbf{a}_{\mathrm{RIS}}^{\mathrm{H}}\left(\vartheta_{x,\ell}, \vartheta_{y,\ell}\right) \quad (4)$$

where β_{RB} and $\beta_{\mathrm{UR},\ell}$ denote the channel gain coefficients of the two segmented subchannels, respectively, ψ_{BS} and $\psi_{\mathrm{UE},\ell}$ denote the pointing directions of the beams at the Base Station (BS) and User Equipment (UE) ends, respectively. $\bar{\vartheta}_x$ and $\bar{\vartheta}_y$ are the azimuth and pitch angles of the beam incidence angle of the RIS in the BS direction, respectively, and $\vartheta_{x,\ell}$ and $\vartheta_{y,\ell}$ are the azimuth and pitch angles of the beam reflection angle of the RIS toward the UE direction, respectively. It is important to note that since the RIS is deployed in space beforehand, its location does not move. For the same RIS, the parameters between the BS and the RIS do not change. As the UE end, the vehicle user is in constant movement and needs to be tracked in real time, so the parameters of the UE end and RIS are time-varying.

From [39], the gain coefficients can be expressed as a function of distance dependence, then the gain coefficients β_{RB} and $\beta_{\mathrm{UR},\ell}$ of the two segmented subchannels can be expressed as a function of their link distance, respectively

$$\beta_{\mathrm{RB}} = \beta d_{\mathrm{RB}}^{-1} e^{j\frac{2\pi}{\lambda}d_{\mathrm{RB}}} = \beta d_{\mathrm{RB}}^{-1} e^{j\frac{2\pi f_c}{c}d_{\mathrm{RB}}} \quad (5)$$

$$\beta_{\mathrm{UR},\ell} = \beta d_{\mathrm{UR},\ell}^{-1} e^{j\frac{2\pi}{\lambda}d_{\mathrm{UR},\ell}} = \beta d_{\mathrm{UR},\ell}^{-1} e^{j\frac{2\pi f_c}{c}d_{\mathrm{UR},\ell}} \quad (6)$$

where their distances are taken for each segmented path, d_{RB} is the distance between BS and RIS, and $d_{\mathrm{UR},\ell}$ is the distance between RIS and UE. Also note that for the same RIS, d_{RB} is a fixed value, while $d_{\mathrm{UR},\ell}$ is time-varying. β is referenced to the channel power gain at a distance of 1 m. Assuming that the reference power gain factor β is known, for the same RIS, the channel gain coefficient β_{RB} of the BS-RIS path is a fixed value, and the estimated channel gain coefficient $\beta_{\mathrm{UR},\ell}$ is equal to the estimated distance $d_{\mathrm{UR},\ell}$. The tracking model can be further simplified depending on this conclusion.

$\mathbf{a}_{\mathrm{BS}}(\psi_{\mathrm{BS}})$ and $\mathbf{a}_{\mathrm{UE}}(\psi_{\mathrm{UE},\ell})$ denote the array response vectors at the BS and UE ends, respectively. Since the ULA arrays are used at both ends, the array response vectors can be specifically expressed as

$$\mathbf{a}_{\mathrm{BS}}\left(\psi_{\mathrm{BS}}\right) = \frac{1}{\sqrt{N_{\mathrm{BS}}}}\left[1, e^{j\psi_{\mathrm{BS}}}, \cdots, e^{j(N_{\mathrm{BS}}-1)\psi_{\mathrm{BS}}}\right]^{\mathrm{T}} \quad (7)$$

$$\mathbf{a}_{\mathrm{UE}}\left(\psi_{\mathrm{UE},\ell}\right) = \frac{1}{\sqrt{N_{\mathrm{UE}}}}\left[1, e^{j\psi_{\mathrm{UE},\ell}}, \cdots, e^{j(N_{\mathrm{UE}}-1)\psi_{\mathrm{UE},\ell}}\right]^{\mathrm{T}} \quad (8)$$

Both the BS and the user are equipped with MIMO antennas. The transceivers all have estimated angles, and the beamformer pointing direction will be adjusted to these angles. By indicating the pointing direction of the receiver combiner and transmitting beamformer by $\bar{\psi}_{\mathrm{UE},\ell}$ and $\bar{\psi}_{\mathrm{BS}}$, the directional beamformers for the estimated angles can be expressed as

$$\mathbf{w}\left(\overline{\psi}_{\mathrm{UE},\ell}\right) = \frac{1}{\sqrt{N_{\mathrm{UE}}}}\left[1, e^{j\overline{\psi}_{\mathrm{UE},\ell}}, \cdots, e^{j(N_{\mathrm{UE}}-1)\overline{\psi}_{\mathrm{UE},\ell}}\right]^{\mathrm{T}} \quad (9)$$

$$\mathbf{f}\left(\overline{\psi}_{\mathrm{BS}}\right) = \frac{1}{\sqrt{N_{\mathrm{BS}}}}\left[1, e^{j\overline{\psi}_{\mathrm{BS}}}, \cdots, e^{j(N_{\mathrm{BS}}-1)\overline{\psi}_{\mathrm{BS}}}\right]^{\mathrm{T}} \quad (10)$$

$\mathbf{a}_{\mathrm{RIS}}(\bar{\vartheta}_x, \bar{\vartheta}_y)$ and $\mathbf{a}_{\mathrm{RIS}}(\vartheta_{x,\ell}, \vartheta_{y,\ell})$ represent the array response of the RIS from the incident direction at the BS end and the reflected direction toward the UE end, respectively. Where, $\mathbf{a}_{\mathrm{RIS}}(\vartheta_{x,\ell}, \vartheta_{y,\ell})$ is time-varying and $\mathbf{a}_{\mathrm{RIS}}(\bar{\vartheta}_x, \bar{\vartheta}_y)$ is a fixed value for the same RIS. The array responses of the UPA are expressed separately as

$$\mathbf{a}_{\mathrm{RIS}}\left(\bar{\vartheta}_x, \bar{\vartheta}_y\right) = \mathbf{a}_x\left(\bar{\vartheta}_x\right) \otimes \mathbf{a}_y\left(\bar{\vartheta}_y\right) \quad (11)$$

$$\mathbf{a}_{\mathrm{RIS}}\left(\vartheta_{x,\ell}, \vartheta_{y,\ell}\right) = \mathbf{a}_x\left(\vartheta_{x,\ell}\right) \otimes \mathbf{a}_y\left(\vartheta_{y,\ell}\right) \quad (12)$$

where $\otimes$ represents the Kronecker product. The above two equations are further expanded and expressed as

$$\begin{aligned}&\mathbf{a}_{\mathrm{RIS}}\left(\overline{\vartheta}_x, \overline{\vartheta}_y\right)\\ &= \frac{1}{\sqrt{N_{\mathrm{RIS}}}}\left[1, e^{j\pi\cos\bar{\vartheta}_y}, \cdots, e^{j(N_x-1)\pi\cos\bar{\vartheta}_y}\right]^{\mathrm{T}}\\ &\otimes\left[1, e^{j\pi\sin\overline{\vartheta}_x\cos\overline{\vartheta}_y}, \cdots, e^{j(N_y-1)\pi\sin\overline{\vartheta}_x\cos\overline{\vartheta}_y}\right]^{\mathrm{T}} \quad (13)\end{aligned}$$

$$\begin{aligned}&\mathbf{a}_{\mathrm{RIS}}\left(\vartheta_{x,\ell}, \vartheta_{y,\ell}\right)\\ &= \frac{1}{\sqrt{N_{\mathrm{RIS}}}}\left[1, e^{j\pi\cos\vartheta_{y,\ell}}, \cdots, e^{j(N_x-1)\pi\cos\vartheta_{y,\ell}}\right]^{\mathrm{T}} \quad (14)\\ &\otimes\left[1, e^{j\pi\sin\vartheta_{x,\ell}\cos\vartheta_{y,\ell}}, \cdots, e^{j(N_y-1)\pi\sin\vartheta_{x,\ell}\cos\vartheta_{y,\ell}}\right]^{\mathrm{T}}\end{aligned}$$

Based on the channel model of the two segmented subchannels, the cascaded channel model can be constructed, expressed as

$$\mathbf{H}_\ell = \mathbf{H}_{\mathrm{UR},\ell}\boldsymbol{\Omega}_\ell\mathbf{H}_{\mathrm{RB}} \quad (15)$$

where $\boldsymbol{\Omega}_\ell$ represents the diagonal phase shift matrix of the RIS. This parameter reflects that RIS can artificially regulate each reflecting unit in the RIS array, change the amplitude and phase shift of the incident signal, and then reflect the signal out, so as to achieve the purpose of regulating the wireless channel. It can be specifically expressed as

$$\boldsymbol{\Omega}_\ell = \mathrm{diag}\left(\gamma_1\omega_{1,\ell}, \cdots, \gamma_{N_{\mathrm{RIS}}}\omega_{N_{\mathrm{RIS}},\ell}\right) \quad (16)$$

where $\mathrm{diag}(\cdot)$ denotes the diagonal matrix; $\omega_{n,\ell}$ is the phase shift parameter; and $\gamma_n \in [0,1]$ is the reflection coefficient. In practice, signal reflection will inevitably bring loss, and complete reflection cannot be achieved. For simplifying model considerations, most studies set the reflection coefficient to 1, that is, $\gamma_n = 1$ [40, 41]. Then the diagonal phase shift matrix can be expressed as

$$\boldsymbol{\Omega}_\ell = \mathrm{diag}\left(\boldsymbol{\omega}_\ell\right) \quad (17)$$

where $\boldsymbol{\omega}_\ell = [\omega_{1,\ell}, \cdots, \omega_{N_{\mathrm{RIS}},\ell}]$. The high dimensional nature of RIS and the iterative nature of the dynamic filter tracking algorithm make the complexity high, requiring a passive beamforming (PBF) scheme for RIS. The PBF scheme of RIS in time slot ℓ can be expressed as

$$\boldsymbol{\omega}_\ell = \mathbf{a}_{\mathrm{RIS}}\left(\hat{\vartheta}_{x,\ell-1}, \hat{\vartheta}_{y,\ell-1}\right) \odot \mathbf{a}_{\mathrm{RIS}}^{\mathrm{H}}\left(\bar{\vartheta}_x, \bar{\vartheta}_y\right) \quad (18)$$

where $\odot$ represents the Khatri-Rao product; $\hat{\vartheta}_{x,\ell-1}$ and $\hat{\vartheta}_{y,\ell-1}$ are estimates of the azimuth and pitch angles of the RIS reflection to the UE direction angle based on the upper time slot, respectively.

Substituting (15) into (1), the received signal at discrete time is written as

$$\begin{aligned}r_\ell &= \sqrt{\rho_\ell}\mathbf{w}^{\mathrm{H}}\mathbf{H}_{\mathrm{UR},\ell}\boldsymbol{\Omega}_\ell\mathbf{H}_{\mathrm{RB}}\mathbf{f}s + \mathbf{w}^{\mathrm{H}}\mathbf{n}_{\mathrm{AWGN}}\\ &= \sqrt{\rho_\ell}\mathbf{w}^{\mathrm{H}}\mathbf{H}_{\mathrm{UR},\ell}\boldsymbol{\Omega}_\ell\mathbf{H}_{\mathrm{RB}}\mathbf{f}s + n_\ell \quad (19)\end{aligned}$$

Substituting (3) and (4) into (19) and expanding, since the gain coefficients β_{RB} and $\beta_{\mathrm{UR},\ell}$ are both constant, the signal expression can be written in detail as

$$\begin{aligned}r_\ell &= \sqrt{\rho_\ell}\mathbf{w}^{\mathrm{H}}\left(\beta_{\mathrm{UR},\ell}\mathbf{a}_{\mathrm{UE}}\left(\psi_{\mathrm{UE},\ell}\right)\mathbf{a}_{\mathrm{RIS}}^{\mathrm{H}}\left(\vartheta_{x,\ell}, \vartheta_{y,\ell}\right)\right)\\ &\cdot\boldsymbol{\Omega}_\ell\left(\beta_{\mathrm{RB}}\mathbf{a}_{\mathrm{RIS}}\left(\bar{\vartheta}_x, \bar{\vartheta}_y\right)\mathbf{a}_{\mathrm{BS}}^{\mathrm{H}}\left(\psi_{\mathrm{BS}}\right)\right)\mathbf{f}s + n_\ell \quad (20)\end{aligned}$$

The time variables in the channel can all eventually be represented by the function $\psi_{\mathrm{UE},\ell}$ of the beam direction of the reflected path from the RIS to the UE direction, namely $\mathbf{H}_\ell = \mathbf{H}(\psi_{\mathrm{UE},\ell})$. Then it can eventually be rewritten as

$$\begin{aligned}r_\ell &= \sqrt{\rho_\ell}\mathbf{w}^{\mathrm{H}}\left(\bar{\psi}_{\mathrm{UE},\ell}\right)\mathbf{H}_{\mathrm{UR},\ell}\left(\psi_{\mathrm{UE},\ell}\right)\\ &\cdot\boldsymbol{\Omega}_\ell\left(\hat{\psi}_{\mathrm{UE},\ell}\right)\mathbf{H}_{\mathrm{RB}}\left(\psi_{\mathrm{BS}}\right)\mathbf{f}\left(\bar{\psi}_{\mathrm{BS}}\right)s + n_\ell \quad (21)\end{aligned}$$

where, for the same RIS case, ψ_{BS} is a fixed value, and the final observed signal is a time-varying signal related to $\psi_{\mathrm{UE},\ell}$. As shown in Fig. 2, the RSU height is h_{RSU} and the RIS height is h_{RIS}. At discrete time ℓ, the coordinates of the vehicle in the moving direction (x-axis) are x_ℓ and the coordinates of the vehicle to the RSU side curb direction (y-axis) are y_ℓ. The angles of the RIS incident and reflected beam directions are decomposed into the azimuthal angle in the horizontal plane and the pitch angle in the vertical plane, and then the azimuthal and pitch angles in the incident and reflected directions are defined as

$$\sin\bar{\vartheta}_x = x_{\mathrm{RIS}}\left(x_{\mathrm{RIS}}^2 + y_{\mathrm{RIS}}^2\right)^{-\frac{1}{2}} \quad (22)$$

$$\cos\bar{\vartheta}_y = \left(x_{\mathrm{RIS}}^2 + y_{\mathrm{RIS}}^2\right)^{\frac{1}{2}}\left(x_{\mathrm{RIS}}^2 + y_{\mathrm{RIS}}^2 + \left(h_{\mathrm{RSU}} - h_{\mathrm{RIS}}\right)^2\right)^{-\frac{1}{2}} \quad (23)$$

$$\sin\vartheta_{x,\ell} = \left(x - x_{\mathrm{RIS}}\right)\left[\left(x - x_{\mathrm{RIS}}\right)^2 + \left(y - y_{\mathrm{RIS}}\right)^2\right]^{-\frac{1}{2}} \quad (24)$$

$$\cos\vartheta_{y,\ell} = \left[\left(x - x_{\mathrm{RIS}}\right)^2 + \left(y - y_{\mathrm{RIS}}\right)^2\right]^{\frac{1}{2}}$$

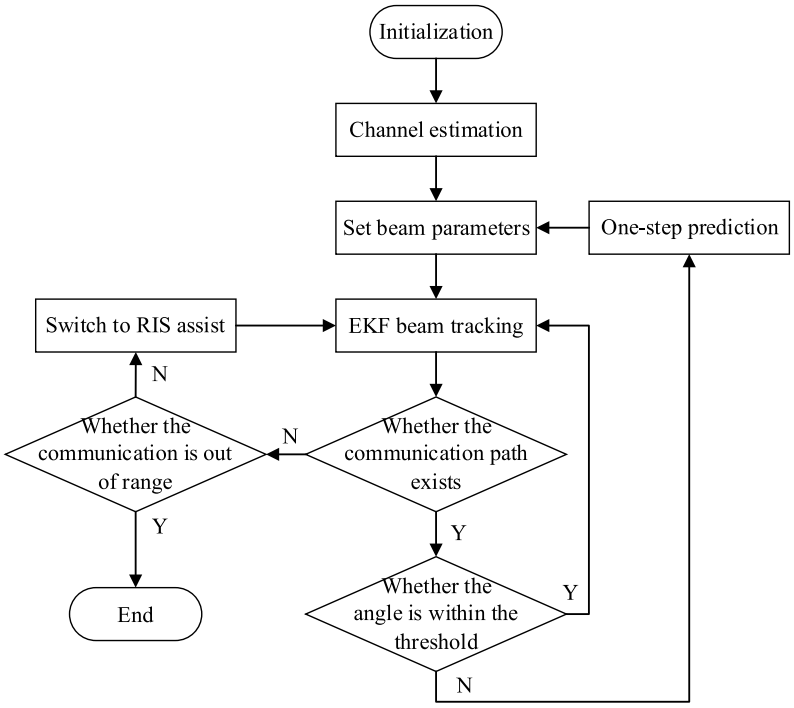

FIGURE 3. Beam tracking process.

$$\cdot \left[(x - x_{\text{RIS}})^2 + (y - y_{\text{RIS}})^2 + h_{\text{RIS}}^2\right]^{-\frac{1}{2}} \tag{25}$$

The beam angle ψ_{BS} in the incident direction and the beam angle $\psi_{\text{UE},\ell}$ in the reflected direction can be approximated by the azimuth and pitch angle respectively in the corresponding directions as follows [42]

$$\begin{aligned} \psi_{\text{BS}} &= \pi \sin\bar{\theta}_x \cos\bar{\theta}_y \\ &= \pi x_{\text{RIS}} \left(x_{\text{RIS}}^2 + y_{\text{RIS}}^2 + (h_{\text{RSU}} - h_{\text{RIS}})^2\right)^{-\frac{1}{2}} \end{aligned} \tag{26}$$

$$\begin{aligned} \psi_{\text{UE},\ell} &= \pi \sin\vartheta_{x,\ell} \cos\vartheta_{y,\ell} = \pi (x - x_{\text{RIS}}) \\ &\left[(x - x_{\text{RIS}})^2 + (y - y_{\text{RIS}})^2 + h_{\text{RIS}}^2\right]^{-\frac{1}{2}} \end{aligned} \tag{27}$$

3. RIS-ASSISTED EKF BEAM TRACKING

3.1. RIS-Assisted Beam Tracking Process

In the mmWave IoV scenario, V2I beam tracking of RSU to IoV users is carried out based on the EKF algorithm. And RIS assistance is introduced to switch to the cascaded channel of RIS to continue beam tracking when the direct connection channel is disconnected. The EKF algorithm runs on the RSU side. In this way, RSU can predict the motion trajectory of the vehicle according to the state information, so as to achieve beam tracking. The tracking process is shown in Fig. 3. Based on the IoV scenario, the vehicle user broadcasts its own status information to other surrounding vehicle users and RSU, it is assumed that the RSU can obtain the vehicle status information at the previous moment. In this paper, we focus on the beam tracking process, so we assume that the channel estimation has been completed to establish the communication link in order to focus on the beam tracking process.

First, the parameters are initialized, and channel estimation is performed to establish the connection. Then, the EKF algorithm is used for continuous beam tracking. After completing the five-step process of EKF in each iteration, the existence of the direct connection LOS path is detected. If the direct connection path exists, the beam threshold detection mechanism is executed. If it is within the set threshold, the next EKF iteration is performed. If it is not within the threshold, the previous moment's state information is used to make a one-step prediction, correct the tracking variables, and perform EKF beam tracking again. In general, the threshold should be set so that the absolute difference of the beam angle is less than or equal to the half beamwidth. This ensures good communication quality while leaving space for beam adjustment, so that a large number of errors are not accumulated during the beam adjustment process, leading to communication disconnection.

If the directly connected LOS path does not exist, it detects whether it is out of communication range. Out of the coverage range of the RSU currently communicating ends the communication and tries to establish a connection with a new RSU in range. If the communication range is not exceeded, it is judged that the LOS path is blocked by an obstacle, probably by a large vehicle or an overhead obstacle in the same scene that blocks the communication link. In this case, the RIS-assisted VLOS path is switched for temporary communication [43]. The EKF beam tracking continues based on the cascaded channel of the BS-RIS-UE. At this point, it is still necessary to detect the presence of LOS paths at regular intervals. This is because in high-speed moving scenarios, although the possibility of link

disconnection due to obstacles is higher, thanks to the high-speed moving situation, such blocking usually does not last too long. Considering that the tracking performance and signal transmission quality of the direct connection channel are higher than those of the cascaded channel, it is necessary to switch back to the direct connection LOS path for communication again when the direct connection LOS path is no longer blocked. Therefore, considering that this RIS-assisted temporary beam tracking does not last long, no threshold detection mechanism is added to the RIS-assisted beam tracking to suppress the accumulated errors of the EKF algorithm. And it also does not consider the case that the continuous tracking is too long, which leads to the accumulation of errors to a certain extent and causes the communication quality to deteriorate and further disconnects the communication.

3.2. RIS-Assisted EKF Beam Tracking Algorithm

This paper focuses on the case where the LOS path is blocked, disconnected, and switched to the RIS-assisted VLOS path for beam tracking.

The state model is constructed based on position and velocity. The position coordinates x_ℓ, y_ℓ, and velocity v_ℓ of the current tracking user at discrete time ℓ are used as the tracking objects. The channel gain of the subchannel can be obtained by estimating the distance approximation. Then the state observation vector $\mathbf{t}_\ell$ is defined as

$$\mathbf{t}_\ell = [x_\ell, y_\ell, v_\ell]^{\mathrm{T}} \tag{28}$$

At this point, the state observation vector $\mathbf{t}_0 = [x_0, y_0, v_0]^{\mathrm{T}}$ at the initial moment can be considered to have been acquired by the RSU. In practice, the tracking estimate before the LOS direct connection path is disconnected can be extended, or a more accurate initial connection can be re-established by the channel estimation method.

The system state space equation can be expressed as

$$\mathbf{t}_\ell = \mathbf{S}\mathbf{t}_{\ell-1} + \mathbf{w}_{\ell-1} \tag{29}$$

The equation represents the actual change of the state observation vector. Where, $\mathbf{w}_{\ell-1} \sim \mathcal{CN}(0, \mathbf{Q}_\omega)$ is the noise excitation vector at time $\ell - 1$. According to the change model of state variables, the state transition matrix $\mathbf{S}$ can be expressed as

$$\mathbf{S} = \begin{bmatrix} 1 & 0 & T_s \cos\varphi \\ 0 & 1 & T_s \sin\varphi \\ 0 & 0 & 1 \end{bmatrix} \tag{30}$$

The process noise matrix $\mathbf{Q}_\omega$ in the noise excitation vector is expressed as

$$\mathbf{Q}_\omega = \mathrm{diag}\left[T_s^2\sigma_\omega^2\cos^2\varphi,\ T_s^2\sigma_\omega^2\sin^2\varphi, \sigma_\omega^2\right] \tag{31}$$

where φ is the vehicle steering angle, which takes into account the practical situation, and it takes the value range $[-\pi/2, \pi/2]$; T_s is the measurement period. The error parameter is the hypothetical noise, which is used to represent the variation in the speed of the vehicle, and σ_ω^2 is the variance of the error parameter.

The received signal r_ℓ is used as the system measurement equation. Since the transceivers both have estimated angles, both $\bar{\psi}_{\mathrm{UE},\ell}$ and $\bar{\psi}_{\mathrm{BS}}$ are fixed values. Since both RSU and RIS are static, ψ_{BS} is a fixed value. The PBF scheme of RIS is related to $\hat{\vartheta}_{x,\ell-1}$ and $\hat{\vartheta}_{y,\ell-1}$, so $\hat{\psi}_{\mathrm{UE},\ell}$ is a fixed value. The position relationship is changing due to the constant movement of the vehicle, so $\psi_{\mathrm{UE},\ell}$ is a time variable. Thus, (21) can be re-expressed as a function related only to $\psi_{\mathrm{UE},\ell}$ as follows

$$r_\ell = \mathbf{h}\left(\psi_{\mathrm{UE},\ell}\right) + n_\ell \tag{32}$$

The real and imaginary parts in the actual calculation need to be calculated separately. To facilitate the state prediction and update process in the same domain, (32) is rewritten in the real domain as

$$\tilde{\mathbf{r}}_\ell = \tilde{\mathbf{h}}\left(\psi_{\mathrm{UE},\ell}\right) + \tilde{\mathbf{n}}_\ell \tag{33}$$

All the variables contained in (33) are reexpressed in the real number field as

$$\tilde{\mathbf{r}}_\ell = \left[r_\ell^{re}, r_\ell^{im}\right]^{\mathrm{T}} \tag{34}$$

$$\tilde{\mathbf{h}}\left(\psi_{\mathrm{UE},\ell}\right) = \left[\mathbf{h}^{re}\left(\psi_{\mathrm{UE},\ell}\right), \mathbf{h}^{im}\left(\psi_{\mathrm{UE},\ell}\right)\right]^{\mathrm{T}} \tag{35}$$

$$\tilde{\mathbf{n}}_\ell = \left[n_\ell^{re}, n_\ell^{im}\right]^{\mathrm{T}} \tag{36}$$

The basic idea of EKF is to linearize the nonlinear system by Taylor series approximation and then perform KF. In order to linearize the measurement process for EKF, the function $\psi_{\mathrm{UE},\ell}$ of the direction of the beam reflected from the RIS to the UE at the moment ℓ is defined as a function of the state vector according to (27), expressed as

$$\begin{aligned}\psi_{\mathrm{UE},\ell} &= \pi\left(x - x_{\mathrm{RIS}}\right)\left[\left(x - x_{\mathrm{RIS}}\right)^2 + \left(y - y_{\mathrm{RIS}}\right)^2 + h_{\mathrm{RIS}}^2\right]^{-\frac{1}{2}} \\ &\doteq g(\mathbf{t}_\ell)\end{aligned} \tag{37}$$

At this point, (33) can be reexpressed as a function related to $g(\mathbf{t}_\ell)$ as follows

$$\tilde{\mathbf{r}}_\ell = \tilde{\mathbf{h}}\left(g\left(\mathbf{t}_\ell\right)\right) + \tilde{\mathbf{n}}_\ell \tag{38}$$

Then, the first-order Taylor series of the received signal obtained from the predicted state vector $\hat{\mathbf{t}}_{\ell|\ell-1}$ at moment ℓ is approximately

$$\tilde{\mathbf{r}}_\ell \simeq \tilde{\mathbf{h}}\left(g\left(\hat{\mathbf{t}}_{\ell|\ell-1}\right)\right) + \tilde{\mathbf{G}}_{\ell|\ell-1}\left(\mathbf{t}_\ell - \hat{\mathbf{t}}_{\ell|\ell-1}\right) + \tilde{\mathbf{n}}_\ell \tag{39}$$

where $\hat{\mathbf{t}}_{\ell|\ell-1}$ is an estimate of the observation vector $\mathbf{t}_\ell$ based on the moment $\ell - 1$; $\tilde{\mathbf{h}}(g(\hat{\mathbf{t}}_{\ell|\ell-1}))$ is the Kalman state prediction; and $\tilde{\mathbf{G}}_{\ell|\ell-1}$ is the Jacobi matrix of the channel vector, denoted as

$$\begin{aligned}\tilde{\mathbf{G}}_{\ell|\ell-1} &= \left.\frac{\partial \mathbf{h}\left(g\left(\mathbf{t}\right)\right)}{\partial \mathbf{t}}\right|\mathbf{t} = \hat{\mathbf{t}}_{\ell|\ell-1} \\ &= \begin{bmatrix}\dot{\mathbf{h}}^{re}\left(g\left(\hat{\mathbf{t}}_{\ell|\ell-1}\right)\right) \\ \dot{\mathbf{h}}^{im}\left(g\left(\hat{\mathbf{t}}_{\ell|\ell-1}\right)\right)\end{bmatrix}\dot{g}\left(\hat{\mathbf{t}}_{\ell|\ell-1}\right)\end{aligned} \tag{40}$$

The terms in (40) are expressed as

$$\dot{\mathbf{h}}^{re}\left(\psi_{\mathrm{UE},\ell}\right) \doteq \left.\frac{\partial \mathbf{h}^{re}\left(\psi_{\mathrm{UE}}\right)}{\partial \psi_{\mathrm{UE}}}\right|\psi_{\mathrm{UE}} = \psi_{\mathrm{UE},\ell} \tag{41}$$

$$\dot{\mathbf{h}}^{im}\left(\psi_{\mathrm{UE},\ell}\right) \doteq \left.\frac{\partial \mathbf{h}^{im}\left(\psi_{\mathrm{UE}}\right)}{\partial \psi_{\mathrm{UE}}}\right|_{\psi_{\mathrm{UE}}=\psi_{\mathrm{UE},\ell}} \tag{42}$$

$$\dot{g}\left(\hat{\mathbf{t}}_{\ell|\ell-1}\right) \doteq \frac{\pi\begin{bmatrix}\left(\hat{y}_{\ell|\ell-1}-y_{\mathrm{RIS}}\right)^2+h_{\mathrm{RIS}}^2\\ -\left(\hat{x}_{\ell|\ell-1}-x_{\mathrm{RIS}}\right)\left(\hat{y}_{\ell|\ell-1}-y_{\mathrm{RIS}}\right)\\ \cos\varphi\left[\left(\hat{y}_{\ell|\ell-1}-y_{\mathrm{RIS}}\right)^2+h_{\mathrm{RIS}}^2\right]T_s\end{bmatrix}^{\mathrm{T}}}{\left[\left(\hat{x}_{\ell|\ell-1}-x_{\mathrm{RIS}}\right)^2+\left(\hat{y}_{\ell|\ell-1}-y_{\mathrm{RIS}}\right)^2+h_{\mathrm{RIS}}^2\right]^{\frac{3}{2}}} \tag{43}$$

Equation (43) can be approximated by $\partial x/\partial v \simeq T_s\cos\varphi$ through the following process

$$\frac{\partial g\left(\mathbf{t}\right)}{\partial \mathbf{t}} = \left[\frac{\partial g\left(\mathbf{t}\right)}{\partial x},\frac{\partial g\left(\mathbf{t}\right)}{\partial y},\frac{\partial g\left(\mathbf{t}\right)}{\partial v}\right]\Bigg|_{\mathbf{t}=[x,y,v]^{\mathrm{T}}} \tag{44}$$

Expanding the received signal through the first-order Taylor series approximation, namely (39), we can obtain

$$\tilde{\mathbf{r}}_\ell \simeq \tilde{\mathbf{G}}_{\ell|\ell-1}\mathbf{t}_\ell + \tilde{\mathbf{h}}\left(g\left(\hat{\mathbf{t}}_{\ell|\ell-1}\right)\right) - \tilde{\mathbf{G}}_{\ell|\ell-1}\hat{\mathbf{t}}_{\ell|\ell-1} + \tilde{\mathbf{n}}_\ell \tag{45}$$

Equation (45) is the observation equation after linearization. This equation is put into the KF to perform the dynamic filtering process, instead of using (33), which merely rewrites the real and imaginary parts in the real domain.

The general Kalman iterative process is divided into five iterative steps, with the first two steps being the prediction processes and the last three steps being the correction processes. Dynamic filter tracking is achieved through continuous iterations of the prediction processes and correction processes. The EKF first approximates the nonlinear system linearly and then uses the KF theory to process it. The specific process of KF is shown as follows.

1. State prediction update

$$\hat{\mathbf{t}}_{\ell|\ell-1} = \mathbf{S}\hat{\mathbf{t}}_{\ell-1|\ell-1} \tag{46}$$

where $\mathbf{S}$ is the state transition matrix in (29).

2. Calculate the prior covariance matrix

$$\mathbf{P}_{\ell|\ell-1} = \mathbf{S}\mathbf{P}_{\ell-1|\ell-1}\mathbf{S}^{\mathrm{T}} + \mathbf{Q}_\omega \tag{47}$$

where the covariance matrix is initialized to $\mathbf{P}_{0|0} = \sigma_\varepsilon^2(\mathbf{t}_0\mathbf{t}_0^{\mathrm{T}})$ at the moment 0; σ_ε^2 is the variance of the initial feedback error parameters; and the process noise matrix $\mathbf{Q}_\omega$ is shown in (31).

3. Kalman gain matrix update

$$\mathbf{K}_\ell = \mathbf{P}_{\ell|\ell-1}\tilde{\mathbf{G}}_{\ell|\ell-1}^{\mathrm{T}}\left(\tilde{\mathbf{G}}_{\ell|\ell-1}\mathbf{P}_{\ell|\ell-1}\tilde{\mathbf{G}}_{\ell|\ell-1}^{\mathrm{T}} + \frac{\mathbf{I}_2}{2\rho_\ell}\right)^{-1} \tag{48}$$

where $\mathbf{K}_\ell$ is the Kalman gain matrix in the KF process; $\tilde{\mathbf{G}}_{\ell|\ell-1}$ is the Jacobi matrix; and $\mathbf{I}$ represents the identity matrix.

4. Update the posterior value of system state estimation

$$\hat{\mathbf{t}}_{\ell|\ell} = \hat{\mathbf{t}}_{\ell|\ell-1} + \mathbf{K}_\ell\left(\tilde{\mathbf{r}}_\ell - \tilde{\mathbf{h}}\left(g\left(\hat{\mathbf{t}}_{\ell|\ell-1}\right)\right)\right) \tag{49}$$

The value of this equation is the system estimate we need, containing the predicted user coordinates and speed information for the discrete moment ℓ.

5. Update the posterior covariance matrix

$$\mathbf{P}_{\ell|\ell} = \left(\mathbf{I}_3 - \mathbf{K}_\ell\tilde{\mathbf{G}}_{\ell|\ell-1}\right)\mathbf{P}_{\ell|\ell-1} \tag{50}$$

The above is the completion of one iteration, the data updated, and a new iteration started.

The prediction processes are cycled through with the correction processes to ensure continuous tracking accuracy. After each round of iteration, the presence of the direct connection LOS path needs to be detected. If it does not exist, the next round of RIS-assisted beam tracking of the VLOS path is performed. If it exists, the communication of the VLOS path is ended, and the communication of the direct connection LOS path is resumed.

4. SIMULATION RESULTS AND ANALYSIS

This section presents a simulation analysis of beam tracking with RIS assistance. The main study is the performance of beam tracking on the VLOS path of BS-RIS-UE when the direct connection LOS path is disconnected and switched to RIS assistance. Using Mean Squared Error (MSE) as the performance metric, the previous algorithms were compared with RIS-assisted VLOS beam tracking performance. The performance with different parameter settings after the introduction of RIS is also analyzed. A ULA-based MIMO system is employed, with the spacing between antennas set to $d = \lambda/2$ by default. $f_c = 28\,\mathrm{GHz}$ is specified as the center frequency of the system, and $B = 20\,\mathrm{MHz}$ is specified as its bandwidth. Accordingly, the magnitude of noise power within a specified bandwidth can be computed as:

$$\sigma_n^2 = -174 + 10\lg(20\times 10^6) \simeq -101\,\mathrm{dBm} \tag{51}$$

Given a path loss exponent of $n = 2$ and a time slot period size of $T_s = 10\,\mathrm{ms}$, the vehicle's initial position is initialized at $(-50\,\mathrm{m}, 8.5\,\mathrm{m})$, the RSU height is configured as $h_{\mathrm{RSU}} = 10\,\mathrm{m}$, and the RIS is located at the coordinates $(-25\,\mathrm{m}, 0\,\mathrm{m})$ [44]. When the error parameter is set to follow a Gaussian distribution, its standard deviation is determined as $\sigma_\omega = 10^{-1.5}$ [23, 45]. The distribution characteristics of the initial feedback error parameter are consistent with the aforementioned error parameter, hence the standard deviation of the initial feedback error is $\sigma_\omega = 10^{-1.5}$. Additionally, after normalizing the reference power gain factor, its value is $\tilde{\beta} = 1$. Unless otherwise specified, both transmitting and receiving ends use 16 antennas by default, transmission power is $-20\,\mathrm{dBm}$, and vehicle motion deflection angle and initial vehicle velocity are $\pi/2^7$ and $10\,\mathrm{m/s}$ respectively, and the RIS employs a UPA array of size 4×4 [44]. Table 1 provides the unified simulation parameter settings. Unless otherwise indicated for comparison, these public simulation parameters shall be used as the default configuration.

Figure 4 compares the tracking MSE of the algorithms in [21, 22] and the VLOS path beam tracking algorithm assisted by RIS in this paper. The method proposed in [21] is an EKF algorithm based on an angle and gain tracking model, combined with half-beam threshold adjustment. And the method in [22] is an EKF algorithm with distance, velocity and gain as tracking variables in a two-dimensional scene. To

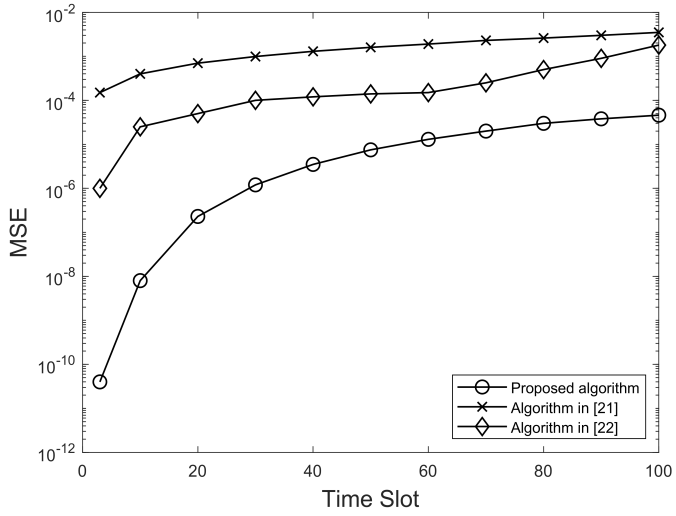

FIGURE 4. Performance comparison of tracking algorithms with and without RIS assistance.

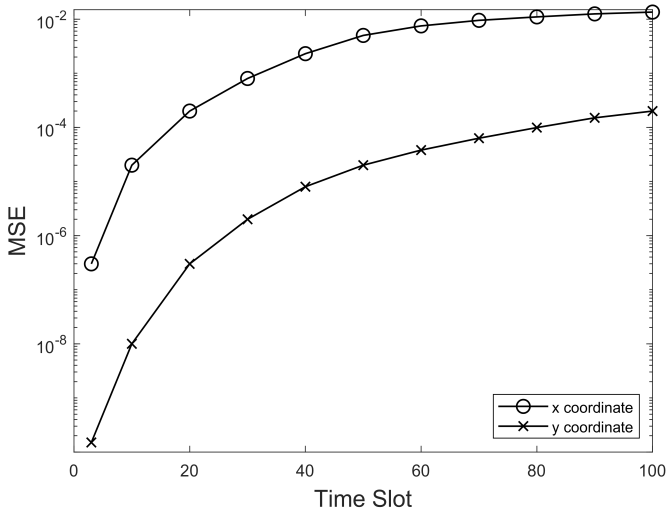

FIGURE 5. Performance comparison of tracking algorithm for x-coordinate and y-coordinate.

TABLE 1. Public simulation parameters.

Simulation parameters	Value
Carrier frequency f_c	28 GHz
Bandwidth B	20 MHz
Noise power σ_n^2	-101 dBm
Path loss index n	2
Time slot period T_s	10 ms
Vehicle initial coordinates (x_0, y_0)	$(-50\,\text{m}, 8.5\,\text{m})$
RSU height h_{RSU}	10 m
RIS height h_{RIS}	10 m
RIS coordinates $(x_{\text{RIS}}, y_{\text{RIS}})$	$(-25\,\text{m}, 0\,\text{m})$
Error parameters σ_ω	$10^{-1.5}$
Initial feedback error σ_ε	$10^{-1.5}$
Power Gain Factor $\tilde{\beta}$	1
Number of antennas at the transmitting end N_{T}	16
Number of antennas at the receiving end N_{R}	16
Number of RIS array elements $N_{\text{RIS}} = N_x N_y$	4×4
Transmitted power p	-20 dBm
Deflection angle φ	$\pi/2^7$
Initial speed v_0	10 m/s

more intuitively compare the differences in MSE performance among various tracking models, the tracked coordinates were converted into beam angles for comparison with the two algorithms. From Fig. 4, it can be observed that the tracking errors of all algorithms exhibit a gradually increasing trend. This arises from the unavoidable linearization error that is introduced in the EKF algorithm, and the error accumulates with each iteration. The results indicate that the tracking error of the method in [21] is the largest, further demonstrating that the novel state evolution and observation model based on position and velocity proposed in [22] is more suitable for V2I communication. From the figure, it can be observed that the simulation curve of the proposed algorithm outperforms the other two algorithms, demonstrating lower MSE and superior tracking performance, while also avoiding the issue of millimeter-wave link interruptions caused by obstructions.

Figure 5 presents a comparison of the MSE performance of RIS-assisted beam tracking along the x-axis and y-axis. It can be observed that the MSE along the x-axis consistently exceeds that along the y-axis, exhibiting significant error throughout the entire time slot range. In contrast, the MSE along the y-axis is markedly lower with a smaller initial error. This discrepancy arises because the primary direction of vehicle motion is along the x-axis, leading to greater positional variations in the x-coordinate and consequently accumulating more tracking error over time. In contrast, variations in the y-coordinate primarily result from steering deviations during vehicle movement, which are smaller in magnitude. Therefore, the tracking error in the y-coordinate is significantly lower than that in the x-coordinate. In the late iteration of time, the curve of the x coordinate has leveled off, while there is still an increase in the tracking error of the y coordinate. This is because the vehicle is in the process of driving towards the RIS, and the closer the distance is, the greater the SNR is, and the better the signal quality is. Therefore, the MSE of the x-coordinate reaches a smoother stage faster. In order to make the simulation concise and intuitive, only the x coordinate with a larger tracking error and as the main direction of advance is used as the simulation object.

Figure 6 compares the performance of the beam tracking with the introduction of RIS assistance when the RIS has different array sizes. As can be seen from the figure, in the early stage of tracking, different RIS sizes all exhibit close tracking errors, but as the number of iterative rounds increases, the errors keep accumulating to show the variability. The tracking error is lower when the RIS array size is $4*4$, while the tracking error is rather larger when the RIS array size is $8*8$. Experimental results indicate that as the size of the RIS array increases, tracking error does not consistently decrease. On the contrary, excessively large arrays may lead to performance degradation. This situation has been studied in detail in [26]. The beam becomes

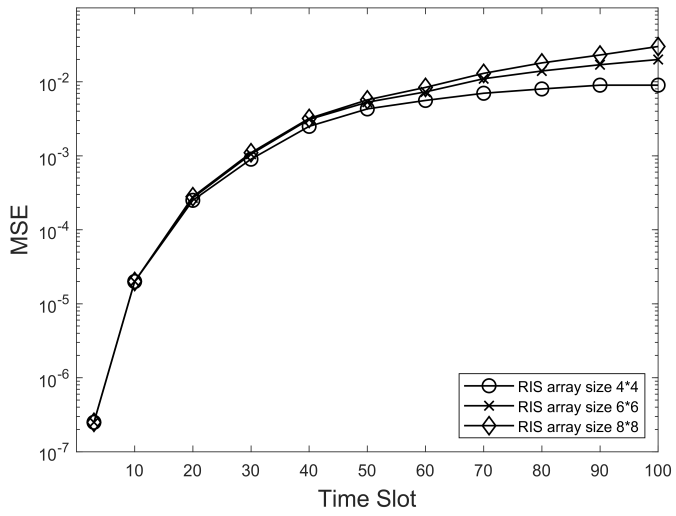

FIGURE 6. Performance comparison of tracking algorithm with different RIS array sizes.

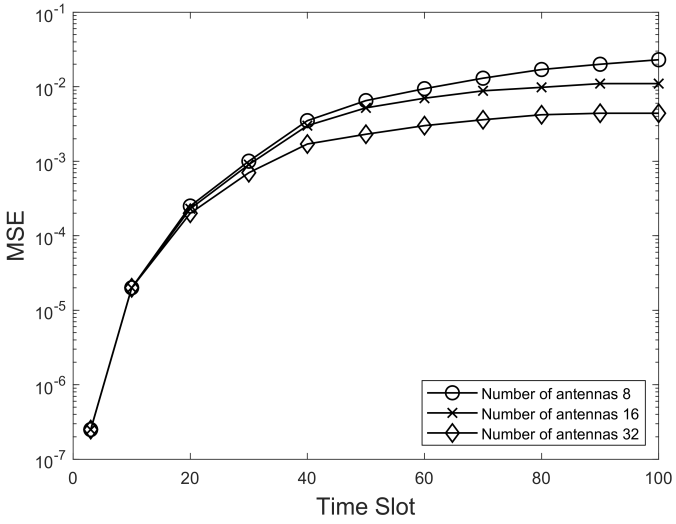

FIGURE 7. Performance comparison of tracking algorithm with different number of antennas.

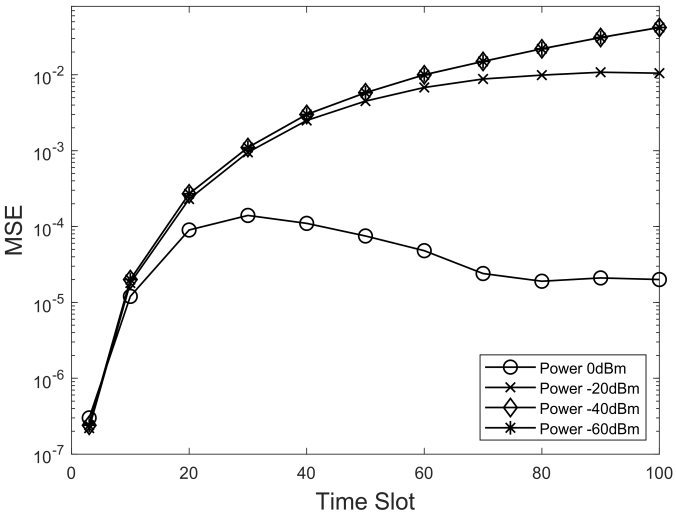

FIGURE 8. Performance comparison of tracking algorithm with different transmission powers.

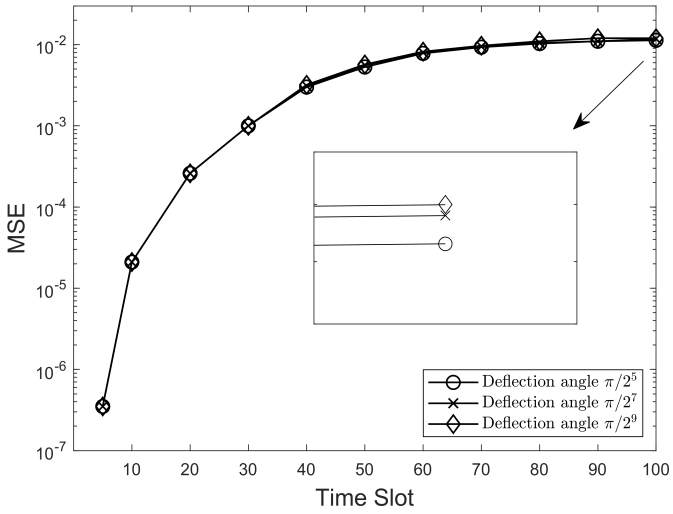

FIGURE 9. Performance comparison of tracking algorithm with different deflection angles.

narrower when more RIS units are configured. The narrower the beam is, the more sensitive it is to angular changes, and the more difficult it is to align the beam in practice. However, the RIS array should not be too small, and too small an array will be less sensitive to changes in Gaussian process noise to achieve accurate tracking.

Figure 7 compares the tracking errors of beam tracking through the RIS-assisted VLOS path for different numbers of antennas. With a different number of antennas, the MSE tends to increase with the accumulation of errors in the EKF algorithm as time advances. When the number of antennas is 32, the error accumulates more slowly and levels off more quickly. While the number of antennas is 8, the error accumulates quickly and shows a tendency to stabilize only in the later part of the tracking time slot. The comparison shows that the tracking error is larger when the number of antennas is 8 and smaller when the number of antennas is 32. That is, a large number of antennas will have a smaller tracking error. As the number of antennas increases, the beam gain will be higher, and the energy will be more concentrated through beamforming. Thus, the signal quality and directivity are continuously improved. Therefore, the simulation results in Fig. 7 are consistent with this rule. However, similar to the RIS array size, the larger the number of antennas is not better. Too narrow a beam will increase the difficulty of tracking, so the number of antennas at the transceiver needs to be set reasonably with reality.

Figure 8 compares the MSE performance of beam tracking through the RIS-assisted VLOS path for different power cases. Among them, the tracking errors show an increasing trend for transmission powers of -20 dBm, -40 dBm, and -60 dBm, and the MSE curves at -40 dBm and -60 dBm almost overlap. This is because the transmission power in both cases is relatively low, making the impact of noise generation quite similar.

According to (2), the SNR in these two cases is closer. When the power is −20 dBm, the accumulation of error is slower than the case of −40 dBm and −60 dBm, with a lower tracking error. When the power is 0 dBm, the tracking error is very low and shows a trend of rising and then falling. This is because when the transmission power is 0 dBm, it will have a large SNR, and the increase in SNR makes the MSE very low. As the vehicle moves to the RIS, the communication distance becomes smaller at the moment, which will show a trend of decreasing tracking error.

Figure 9 shows the tracking performance at different deflection angles. Overall, as the number of time slots increases, the MSE corresponding to all three deflection angles gradually increases. The three curves almost overlap, indicating that the deflection angle does not have much effect on the x coordinate as the forward direction. By zooming in on the local part of the curve in the later stage, it can be observed that when the deflection angle is relatively large, the tracking error is relatively small. However, when the deflection angle is relatively small, the MSE is slightly higher. The reason for this phenomenon is that when the vehicle has the same forward speed, a larger deflection angle will reduce the velocity component in the x-axis direction, thus reducing the tracking error in the x-coordinate direction. Conversely, a smaller deflection angle will result in a larger velocity component in the x-axis, leading to an increase in tracking error. This result is consistent with the rule that "the higher the speed, the worse the tracking effect." It should also be noted that this rule exhibits an opposite trend on the y-axis direction: specifically, as the deflection angle increases, the velocity component in the y-axis increases, thereby leading to a larger tracking error.

Figure 10 compares the tracking errors at different initial velocities. As shown in the figure, the curves show a rising and then decreasing trend, except for the case where the velocity is 10 m/s. According to (2), a smaller spatial distance will have a higher SNR. As the vehicle approaches the RSU quickly, the increasing SNR will suppress or even reduce the tracking error, and it will have a better communication quality. This allows for an earlier performance of the downward trend, even at lower speeds. The faster the vehicle moves, the faster it approaches the RIS, then the faster curve exhibits a downward trend at an earlier time slot. The curve with a velocity of 25 m/s again shows an upward trend in the last 10 time slots. This is because the linearization error introduced by the EKF is still in a constant state of accumulation. When the error reduction due to the increased SNR drops to a trough, the upward trend resumes. It is important to note that it is not the case that the faster the velocity is, the lower the tracking error is. The performance in Fig. 10 is influenced by the SNR that varies with distance. When the effect of distance on SNR is not considered, faster motion speed increases the difficulty of tracking, and lower motion speed results in more accurate tracking performance.

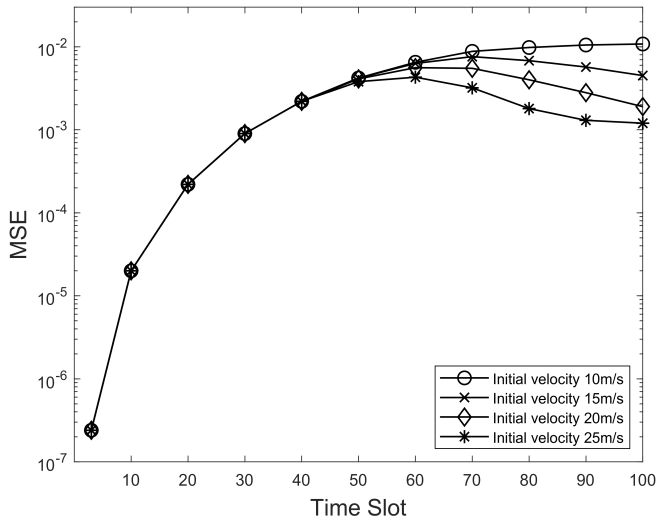

FIGURE 10. Performance comparison of tracking algorithm with different initial velocities.

5. CONCLUSION

Based on the new state model of position and velocity, the RIS-assisted VLOS path beam tracking model in the 3D road scene is derived. A cascade channel model for VLOS path tracking is studied. The RIS-assisted beam tracking process is designed, and the beam tracking under the VLOS path is realized based on the EKF algorithm. The performance of the algorithm under this system model is simulated and analyzed with MSE as the performance index. The simulation results show that the RIS-assisted VLOS beam tracking based on the new state model has lower tracking errors than the conventional scheme, and provides a new solution to the problem of mmWave IoV scenarios that are susceptible to occlusion. However, this paper does not consider the case of multiple RIS-assisted communication, which can be further studied in the future.

Additionally, the research framework proposed in this paper possesses clear engineering application value, enabling the establishment of stable virtual LOS links in obstructed scenarios to enhance beam continuity and communication reliability. With its clear structure and strong modularity, the framework is easily scalable to multi-RIS, multi-user, and real-world measurement environments, demonstrating strong potential for engineering implementation.

ACKNOWLEDGEMENT

This work was supported by the Natural Science Foundation of Fujian Province (Grant No. 2022J011276, and No. 2023I0044), Undergraduate Education and Teaching Research Project of Fujian Province (Grant No. FBJY20240120), High-level Talent Project of Xiamen University of Technology (Grant No. YKJ22030R, and No. YKJ23034R), and Postgraduate Science and Technology Innovation Project of Xiamen University of Technology (Grant No. YKJCX2024143).

REFERENCES

[1] Cao, Y., X. He, C. Yu, and C. Yin, "Reliability and latency of mmWave communications based on blockage avoidance in internet of vehicles," in *2021 13th International Conference on Wireless Communications and Signal Processing (WCSP)*, 1–5, Changsha, China, 2021.

[2] Kwon, D., J. Kim, D. A. Mohaisen, and W. Lee, "Self-adaptive power control with deep reinforcement learning for millimeter-wave internet-of-vehicles video caching," *Journal of Communications and Networks*, Vol. 22, No. 4, 326–337, 2020.

[3] Choi, J., V. Va, N. Gonzalez-Prelcic, R. Daniels, C. R. Bhat, and R. W. Heath, "Millimeter-wave vehicular communication to support massive automotive sensing," *IEEE Communications Magazine*, Vol. 54, No. 12, 160–167, 2016.

[4] Ghosh, J., H. Zhu, and H. Haci, "A novel channel model and optimal beam tracking schemes for mobile millimeter-wave massive MIMO communications," *IEEE Transactions on Vehicular Technology*, Vol. 70, No. 7, 7205–7210, 2021.

[5] Duan, Q., T. Kim, H. Huang, K. Liu, and G. Wang, "AoD and AoA tracking with directional sounding beam design for millimeter wave MIMO systems," in *2015 IEEE 26th Annual International Symposium on Personal, Indoor, and Mobile Radio Communications (PIMRC)*, 2271–2276, Hong Kong, China, 2015.

[6] Blandino, S., J. Senic, C. Gentile, D. Caudill, J. Chuang, and A. Kayani, "Markov multi-beamtracking on 60 GHz mobile channel measurements," *IEEE Open Journal of Vehicular Technology*, Vol. 3, 26–39, 2022.

[7] Palacios, J., D. D. Donno, and J. Widmer, "Tracking mm-Wave channel dynamics: Fast beam training strategies under mobility," in *IEEE INFOCOM 2017 — IEEE Conference on Computer Communications*, 1–9, Atlanta, GA, USA, 2017.

[8] Basharat, S., S. A. Hassan, H. Pervaiz, A. Mahmood, Z. Ding, and M. Gidlund, "Reconfigurable intelligent surfaces: Potentials, applications, and challenges for 6G wireless networks," *IEEE Wireless Communications*, Vol. 28, No. 6, 184–191, 2021.

[9] Pan, C., H. Ren, K. Wang, J. F. Kolb, M. Elkashlan, M. Chen, M. D. Renzo, Y. Hao, J. Wang, A. L. Swindlehurst, X. You, and L. Hanzo, "Reconfigurable intelligent surfaces for 6G systems: Principles, applications, and research directions," *IEEE Communications Magazine*, Vol. 59, No. 6, 14–20, 2021.

[10] Zhao, Y., J. Zhang, and B. Ai, "Applications of reconfigurable intelligent surface in smart high-speed railway communications," *ZTE Technology Journal*, Vol. 27, No. 4, 36–43, 2021.

[11] Zhao, Y. and M. Jian, "Applications and challenges of reconfigurable intelligent surface for 6G networks," *Radio Communications Technology*, Vol. 47, No. 6, 679–691, 2021.

[12] Kurma, S., M. Katwe, K. Singh, C. Pan, S. Mumtaz, and C.-P. Li, "RIS-empowered MEC for URLLC systems with digital-twin-driven architecture," *IEEE Transactions on Communications*, Vol. 72, No. 4, 1983–1997, 2024.

[13] Zhu, Q., Y. Gao, Y. Xiao, M. Xiao, and S. Mumtaz, "Intelligent reflecting surface aided wireless networks: Dynamic user access and system sum-rate maximization," *IEEE Transactions on Communications*, Vol. 70, No. 4, 2870–2881, 2022.

[14] Yuan, J., G. C. Alexandropoulos, E. Kofidis, T. L. Jensen, and E. de Carvalho, "Channel tracking for RIS-enabled multi-user SIMO systems in time-varying wireless channels," in *2022 IEEE International Conference on Communications Workshops (ICC Workshops)*, 145–150, Seoul, Republic of Korea, 2022.

[15] Ai, Y., F. A. P. de Figueiredo, L. Kong, M. Cheffena, S. Chatzinotas, and B. Ottersten, "Secure vehicular communications through reconfigurable intelligent surfaces," *IEEE Transactions on Vehicular Technology*, Vol. 70, No. 7, 7272–7276, 2021.

[16] Yang, L. and W. Zhang, "Beam tracking and optimization for UAV communications," *IEEE Transactions on Wireless Communications*, Vol. 18, No. 11, 5367–5379, 2019.

[17] Seo, J., Y. Sung, G. Lee, and D. Kim, "Training beam sequence design for millimeter-wave MIMO systems: A POMDP framework," *IEEE Transactions on Signal Processing*, Vol. 64, No. 5, 1228–1242, 2016.

[18] Liu, G., H. Duan, and J. Hou, "Beam tracking based on second-order extended Kalman filter theory in millimeter wave communication systems," *Journal of Chongqing University of Posts and Telecommunications(Natural Science Edition)*, Vol. 33, No. 3, 412–419, 2021.

[19] Xin, X. and Y. Yang, "Research on extended Kalman filter algorithm for millimeter wave beam tracking," *Journal of Microwaves*, Vol. 35, No. 6, 16–20, 2019.

[20] Zhang, C., D. Guo, and P. Fan, "Tracking angles of departure and arrival in a mobile millimeter wave channel," in *2016 IEEE International Conference on Communications (ICC)*, 1–6, Kuala Lumpur, Malaysia, 2016.

[21] Va, V., H. Vikalo, and R. W. Heath, "Beam tracking for mobile millimeter wave communication systems," in *2016 IEEE Global Conference on Signal and Information Processing (GlobalSIP)*, 743–747, Washington, DC, USA, 2016.

[22] Shaham, S., M. Ding, M. Kokshoorn, Z. Lin, S. Dang, and R. Abbas, "Fast channel estimation and beam tracking for millimeter wave vehicular communications," *IEEE Access*, Vol. 7, 141 104–141 118, 2019.

[23] Hyun, S.-H., J. Song, K. Kim, J.-H. Lee, and S.-C. Kim, "Adaptive beam design for V2I communications using vehicle tracking with extended Kalman filter," *IEEE Transactions on Vehicular Technology*, Vol. 71, No. 1, 489–502, 2022.

[24] Cai, P., J. Zong, X. Luo, Y. Zhou, S. Chen, and H. Qian, "Downlink channel tracking for intelligent reflecting surface-aided FDD MIMO systems," *IEEE Transactions on Vehicular Technology*, Vol. 70, No. 4, 3341–3353, 2021.

[25] Teng, B., X. Yuan, R. Wang, and S. Jin, "Bayesian user tracking for reconfigurable intelligent surface aided mmWave MIMO system," in *2022 IEEE 12th Sensor Array and Multichannel Signal Processing Workshop (SAM)*, 201–205, Trondheim, Norway, 2022.

[26] Zhang, P., J. Zhang, H. Xiao, H. Du, D. Niyato, and B. Ai, "RIS-aided 6G communication system with accurate traceable user mobility," *IEEE Transactions on Vehicular Technology*, Vol. 72, No. 2, 2718–2722, 2023.

[27] Tian, Y., B. Xiao, X. Wang, Y. H. Kho, C. Zhu, W. Li, Q. Li, and X. Hu, "Opportunistic RIS-assisted rate splitting transmission in coordinated multiple points networks," *Computer Communications*, Vol. 202, 23–32, 2023.

[28] Wang, X., H. Zhang, Y. Tian, and V. C. M. Leung, "Modeling and analysis of aerial base station-assisted cellular networks in finite areas under LoS and NLoS propagation," *IEEE Transactions on Wireless Communications*, Vol. 17, No. 10, 6985–7000, 2018.

[29] Xiao, B., Y. Tian, W. Li, Y. H. Kho, X. Wang, C. Zhu, and H. Liu, "Performance analysis of adaptive RIS-assisted clustering strategies in downlink communication systems," *IEEE Internet of Things Journal*, Vol. 10, No. 5, 4520–4530, 2023.

[30] Wang, X., H. Zhang, K. J. Kim, Y. Tian, and A. Nallanathan, "Performance analysis of cooperative aerial base station-assisted networks with non-orthogonal multiple access," *IEEE Transactions on Wireless Communications*, Vol. 18, No. 12, 5983–5999, 2019.

[31] Wang, X., H. Zhang, H. Yang, Y. Tian, C. Zhu, and A. Nallanathan, "A non-orthogonal cross-tier joint transmission design for clustered ABS-assisted networks," *IEEE Transactions on Wireless Communications*, Vol. 23, No. 4, 3361–3376, 2024.

[32] Wang, Y., L. Yang, and T. Zhang, "Channel estimation based on compressive sensing in RIS-assisted millimeter wave system," *Journal of Computer Applications*, Vol. 42, No. 12, 3870–3875, 2022.

[33] Ghafoor, K. Z., L. Kong, S. Zeadally, A. S. Sadiq, G. Epiphaniou, M. Hammoudeh, A. K. Bashir, and S. Mumtaz, "Millimeter-wave communication for internet of vehicles: Status, challenges, and perspectives," *IEEE Internet of Things Journal*, Vol. 7, No. 9, 8525–8546, 2020.

[34] Mejri, A., M. Hajjaj, S. Hasnaoui, and R. Bouallegue, "Singular value thresholding based adaptive approach for hybrid beamforming in mmWave massive MIMO-OFDM transmitters," in *2018 26th International Conference on Software, Telecommunications and Computer Networks (SoftCOM)*, 1–5, Split, Croatia, 2018.

[35] Li, H., Y. Zhang, J. Xi, and W. Guo, "3D beam tracking method based on reconfigurable intelligent surface assistant for blocking channel," in *2021 36th Youth Academic Annual Conference of Chinese Association of Automation (YAC)*, 684–689, Nanchang, China, 2021.

[36] Mi, L., X. He, and L. Sun, "Research on sparse adaptive cascade channel estimation method based on compressed sensing in RIS assisted wireless system," *Journal of Signal Processing*, Vol. 38, No. 10, 2173–2179, 2022.

[37] Zeng, R. and X. Hang, "Reconfigurable intelligent surface assist wireless channel estimation algorithm in internet of vehicles environment," *Journal on Communications*, Vol. 43, No. 8, 142–150, 2022.

[38] Qin, Q., L. Gui, P. Cheng, and B. Gong, "Time-varying channel estimation for millimeter wave multiuser MIMO systems," *IEEE Transactions on Vehicular Technology*, Vol. 67, No. 10, 9435–9448, 2018.

[39] Heath, R. W., N. González-Prelcic, S. Rangan, W. Roh, and A. M. Sayeed, "An overview of signal processing techniques for millimeter wave MIMO systems," *IEEE Journal of Selected Topics in Signal Processing*, Vol. 10, No. 3, 436–453, 2016.

[40] Wang, P., J. Fang, H. Duan, and H. Li, "Compressed channel estimation for intelligent reflecting surface-assisted millimeter wave systems," *IEEE Signal Processing Letters*, Vol. 27, 905–909, 2020.

[41] Chen, J., Y.-C. Liang, H. V. Cheng, and W. Yu, "Channel estimation for reconfigurable intelligent surface aided multi-user mmWave MIMO systems," *IEEE Transactions on Wireless Communications*, Vol. 22, No. 10, 6853–6869, 2023.

[42] Liu, F., W. Yuan, C. Masouros, and J. Yuan, "Radar-assisted predictive beamforming for vehicular links: Communication served by sensing," *IEEE Transactions on Wireless Communications*, Vol. 19, No. 11, 7704–7719, 2020.

[43] Tian, Y., B. Xiao, X. Wang, Y. H. Kho, and C. Tian, "Performance analysis of opportunistic NOMA strategy in uplink coordinated multi-points systems," *Computer Communications*, Vol. 177, 207–212, 2021.

[44] Sun, Y., C.-W. Feng, X.-L. Wang, J.-N. Yuan, and L. Zhang, "Beam tracking based on a new state model for mmWave V2I communication on 3D roads," *Journal of Computers*, Vol. 35, No. 1, 33–50, 2024.

[45] Song, J., J.-H. Lee, S. Noh, and J. Choi, "Millimeter wave reflection pattern codebook design for RIS-assisted V2V communications," *IEEE Transactions on Vehicular Technology*, Vol. 71, No. 6, 6819–6824, 2022.